

Characterization of wildfire NO_x emissions using MODIS fire radiative power and OMI tropospheric NO_2 columns

A. K. Mebust¹, A. R. Russell¹, R. C. Hudman¹, L. C. Valin¹, and R. C. Cohen^{1,2}

¹Department of Chemistry, University of California at Berkeley, Berkeley, California, USA

²Department of Earth and Planetary Science, University of California at Berkeley, Berkeley, California, USA

Received: 14 January 2011 – Published in Atmos. Chem. Phys. Discuss.: 11 February 2011

Revised: 14 June 2011 – Accepted: 14 June 2011 – Published: 22 June 2011

Abstract. We use observations of fire radiative power (FRP) from the Moderate Resolution Imaging Spectroradiometer (MODIS) and tropospheric NO_2 column measurements from the Ozone Monitoring Instrument (OMI) to derive NO_2 wildfire emission coefficients (g MJ^{-1}) for three land types over California and Nevada. Retrieved emission coefficients were 0.279 ± 0.077 , 0.342 ± 0.053 , and $0.696 \pm 0.088 \text{ g MJ}^{-1} \text{ NO}_2$ for forest, grass and shrub fuels, respectively. These emission coefficients reproduce ratios of emissions with fuel type reported previously using independent methods. However, the magnitude of these coefficients is lower than prior estimates. While it is possible that a negative bias in the OMI NO_2 retrieval over regions of active fire emissions is partly responsible, comparison with several other studies of fire emissions using satellite platforms indicates that current emission factors may overestimate the contributions of flaming combustion and underestimate the contributions of smoldering combustion to total fire emissions. Our results indicate that satellite data can provide an extensive characterization of the variability in fire NO_x emissions; 67 % of the variability in emissions in this region can be accounted for using an FRP-based parameterization.

1 Introduction

Emissions from vegetation fires are a significant source of trace gases (e.g. CO, NO_x , VOCs) and particulate matter to the atmosphere (Andreae and Merlet, 2001); formation of secondary pollutants occurs as a result of these emissions with consequences that range from local to global in scale (e.g. Val Martin et al., 2006; Cook et al., 2007; Pfister et al., 2008; Hudman et al., 2009). NO_x ($\text{NO} + \text{NO}_2$) emis-

sions play a major role both in the production of ozone, a monitored pollutant and tropospheric greenhouse gas, and in the regulation of oxidant concentrations. NO_x emissions from biomass and biofuel burning contribute approximately 5.9 Tg N y^{-1} to the atmosphere, roughly 15 % of the global NO_x budget (Denman et al., 2007), with total emissions from wildfires fluctuating from year to year due to interannual variability in fire frequency and intensity. However, there are significant uncertainties associated with biomass burning budgets due to the large uncertainties in NO_x emission factors and global biomass burned. For example, Jaeglé et al. (2005) partitioned yearly GOME satellite NO_2 data to determine budgets for individual NO_x sources in 2000; while a priori and top-down global inventory totals for fire emissions agreed, regional differences of up to 50 % between these two inventories were noted and attributed to uncertainties in regionally resolved NO_x emission factors used in the study. Laboratory studies also indicate that biomass burning NO_x emission factors can vary greatly—even among plants from similar ecosystems or categorized as similar under current emissions inventories, e.g. extratropical forest (McMeeking et al., 2009). These wide variations on regional scales raise questions as to whether existing parameterizations capture the mean emissions from the range of recent fires, and whether a more detailed parameterization could capture some of the variability in emissions.

Biomass burning emissions have generally been estimated using a bottom-up approach (Wiedinmyer et al., 2006):

$$M_X = M_T \times \text{EF}_X \quad (1)$$

where M_X is the mass of a species X emitted by the fire, M_T is the total biomass burned, and EF_X is the empirically measured emission factor (EF) for species X, expressed as the ratio of pollutant mass emitted to the total biomass burned. NO_x emissions vary greatly based on individual fire conditions, such as differences in the flaming vs. smoldering fraction of the fuel burned and its nitrogen content; most NO_x



Correspondence to: R. C. Cohen
(rccohen@berkeley.edu)

EFs used in atmospheric modeling applications are reported with high uncertainties ($\pm 50\%$) as this variability is significant between different biomes and emissions in a given location are attributed to one of only a handful of biome categories (Andreae and Merlet, 2001; Battye and Battye, 2002). NO_x EFs are primarily based on airborne and occasionally local measurements from wildfires or prescribed fires (e.g. Laursen et al., 1992; Goode et al., 2000; Yokelson et al., 2007; Alvarado et al., 2010), or measurements from small fires burned under controlled laboratory conditions (e.g. Goode et al., 1999; Freeborn et al., 2008; Yokelson et al., 2008; McMeeking et al., 2009). Airborne measurements, while precise for a given fire, face obvious limitations with respect to the number and size of fires that can be sampled, limiting their ability to characterize variability in fire emissions on regional scales; these measurements may also exhibit a bias toward emissions from flaming combustion (Andreae and Merlet, 2001; Yokelson et al., 2008; van Leeuwen and van der Werf, 2011). Laboratory fires, on the other hand, do not accurately recreate several characteristics of typical large-scale natural wildfires including size, fuel moisture, flaming and smoldering fractions, and structural and meteorological characteristics, among others. Satellite measurements offer an opportunity to bridge the gap between global analyses that identify a need for representative emission factors at regional scales and observations at the fuel and individual fire level.

In the mass-burned formalism M_T is estimated as

$$M_T = A \times B \times C \quad (2)$$

where A is the burned area, B is the available fuel per unit area, and C is the combustion completeness, or fraction of available fuel that was burned (Seiler and Crutzen, 1980; Wiedinmyer et al., 2006). Poor knowledge of A , B and C leads to large uncertainties in the mass of pollutant emitted, and the lack of temporal and spatial resolution prevents air quality forecasting of individual fires in real time (Ichoku and Kaufman, 2005). In recent literature, a linear relationship between the biomass burned in a fire and the radiative energy released by the fire has been established (Wooster, 2002; Wooster et al., 2005; Freeborn et al., 2008), leading to a new expression of pollutant mass emission:

$$M_X = EC_X \times E_R = K \times EF_X \times E_R \quad (3)$$

where EC_X is an “emission coefficient” (EC) expressed as the mass of pollutant emitted per unit of radiative energy, E_R is the total radiative energy, and K is an empirically measured coefficient with reported uncertainties of approximately 10–15% (Ichoku and Kaufman, 2005; Wooster et al., 2005; Vermote et al., 2009). E_R can be measured remotely and so may have lower uncertainties than estimates of mass burned for larger fires; thus some recent studies of fire emissions have focused on directly establishing EC_X for pollutants of interest (Ichoku and Kaufman, 2005; Freeborn et al.,

2008; Jordan et al., 2008; Vermote et al., 2009). Although NO_x ECs have been measured for small experimental fires (Freeborn et al., 2008), they may not accurately represent emissions for larger scale natural fires, and only a small number of fuel types are represented. Satellite observations with relatively high spatiotemporal resolution provide us the opportunity to directly measure NO_x ECs and to gather statistics of variation among wildfires using observations from a large number of fires.

Here we show that satellite observations of fire activity and NO₂ can establish statistical properties of NO₂ ECs. We evaluate emissions from 1960 fires in California and Nevada over the years 2005–2008 to derive NO₂ ECs for three land cover classes (forest, shrub and grass) by combining NO₂ columns from the Ozone Monitoring Instrument (OMI) aboard NASA’s EOS-Aura satellite, wind vectors from the North American Regional Reanalysis (NARR), and measurements of fire radiative power (FRP) from the Moderate Resolution Imaging Spectroradiometer (MODIS) instrument on NASA’s EOS-Aqua satellite. Although not considered a major contributor to global biomass burning emissions, this region has a number of fires over diverse land types which can aid our understanding of variations in emissions with fuel type. Further, emissions from individual fires in this region can significantly perturb NO_x levels over the natural background, leading to local and regional degradation of air quality (Pfister et al., 2008). We note that in this paper, the phrases “NO₂ emissions” and “NO₂ ECs” refer to emissions and ECs derived from the observed NO₂ columns, and thus represent total NO₂ present in plumes at NO-NO₂ photostationary state, as opposed to direct NO₂ emissions from fires.

2 Datasets

The MODIS instruments reside on the NASA EOS-Terra and EOS-Aqua satellites, measuring spectral radiance from Earth; the MODIS fire detection algorithm employs infrared spectral channels at 4 and 11 μm (Kaufman et al., 1998). We use daytime fire detections at 1 km nominal resolution from the MODIS Aqua Thermal Anomalies Level 2 Collection 5 data product, MYD14 (Giglio et al., 2003). FRP is provided for each fire pixel via an empirical relationship using the 4 μm band brightness temperatures (Kaufman et al., 1998; Justice et al., 2002). Sensitivity studies indicate that the theoretical average standard error associated with this relationship is $\pm 16\%$, and is higher for small fires and lower for more energetic fires (Kaufman et al., 1998). Independent validation by Wooster et al. (2003) using the Bi-spectral InfraRed Detection satellite instrument found that the two instruments agreed to within 15% for some fires but that MODIS underestimates FRP by up to 46% for fires where some of the less intensely radiating fire pixels are not detected by the MODIS algorithm. To identify the primary land

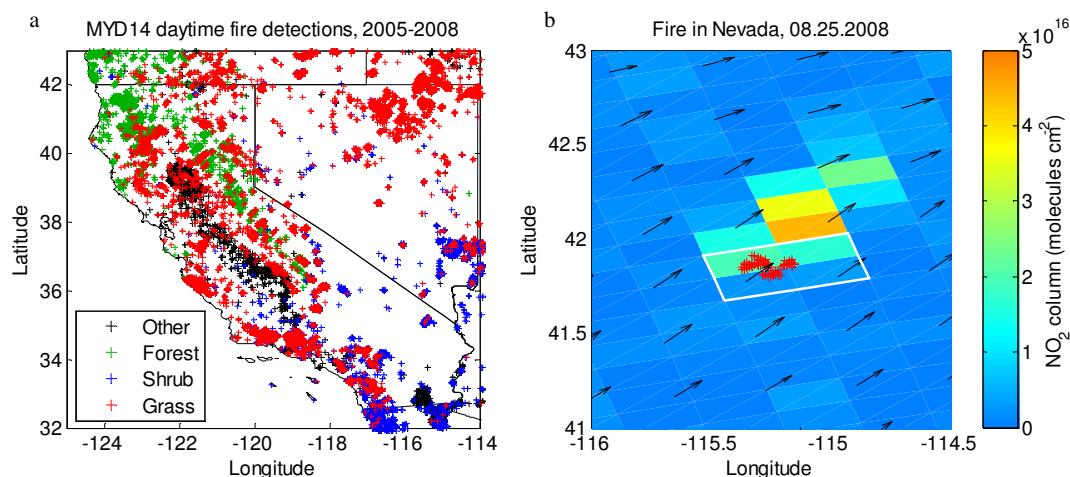


Fig. 1. (a) MODIS fire detections (totaling $\sim 2.8 \times 10^4$ 1 km pixels) from the daytime EOS-Aqua overpass over California and Nevada, for 2005–2008, colored by land type. (b) OMI tropospheric NO₂ column densities (molecules cm⁻²), overlaid with MODIS fire detections (red) and NARR wind vectors (black arrows) for a fire detected in Nevada on 25 August 2008; OMI pixels analyzed for this fire are outlined in white. Average wind speed shown is 8.23 m s^{-1} .

type for each fire pixel we use the MODIS Aqua+Terra Land Cover Level 3 Collection 5 (MCD12Q1) product, which provides yearly land cover classification at $500 \text{ m} \times 500 \text{ m}$ resolution (Friedl et al., 2010).

To measure NO₂ emissions we use tropospheric vertical column densities of NO₂ obtained from the OMI NO₂ standard product (Level 2, Version 1.0.5, Collection 3) available from the NASA Goddard Earth Sciences (GES) Data and Information Services Center (DISC). OMI is a nadir-viewing spectrometer, measuring backscattered solar radiation from earth at UV and visible wavelengths (270–500 nm) with a spectral resolution of $\sim 0.5 \text{ nm}$. OMI employs differential optical absorption spectroscopy (DOAS) to measure NO₂; the tropospheric vertical columns of NO₂ and corresponding standard errors used in this work are retrieved as described by Boersma et al. (2004), Bucsela et al. (2006), and Celarier et al. (2008). With daily global coverage at a spatial resolution of $13 \text{ km} \times 24 \text{ km}$ at nadir, OMI has the highest resolution of any remote instrument measuring NO₂ columns. In this work, only the 40 inner pixels out of 60 total (in the across-track direction) were used, minimizing effects of poor resolution in the outer, larger pixels. OMI pixels with cloud fractions greater than 20% were not included in our analysis to reduce uncertainties associated with cloud cover (Boersma et al., 2002; Celarier et al., 2008).

We use wind fields at 900 hPa ($\sim 1 \text{ km}$) from NARR, a data assimilation system that provides meteorological variables at 32 km horizontal resolution and 45 vertical layers every three hours from 1979–present (Mesinger et al., 2006). MODIS, OMI and NARR data for each fire were collocated in time to within one hour.

3 Methods

We follow the method outlined by Ichoku and Kaufman (2005), which computes regional ECs globally for smoke aerosol, with modifications to calculate ECs for NO₂. We begin with a brief summary of the method presented in the aforementioned study.

Ichoku and Kaufman (2005) first collocated MODIS aerosol pixels and MODIS fire detections. For each MODIS aerosol pixel identified as containing fire, a series of calculations were performed; first, the aerosol optical thickness (AOT) contributed by fire emissions was measured by subtracting the minimum AOT of the aerosol pixel containing fire and the eight surrounding aerosol pixels from the maximum AOT of these same pixels. Next, the authors converted AOT to column mass density. Ichoku and Kaufman (2005) then calculated the wind speed over the pixel and a characteristic length over which the wind must blow to clear the region of aerosol; this was given as the square root of the area of the aerosol pixel. Using this characteristic length and the wind speed to determine the clear time (defined below), the smoke mass emission rate is given as the total mass of aerosol contributed by fire emissions divided by the clear time. Ichoku and Kaufman (2005) then grouped aerosol pixels by their proximity and averaged these values for all pixels in a group.

For fire NO_x emissions, we began by collecting fire detections over California and Nevada and surrounding areas ($31\text{--}44^\circ \text{ N}$, $126\text{--}113^\circ \text{ W}$) from 2005–2008. These fire pixels were assigned a primary fuel type of forest, shrub, grass or “other” (including sparsely vegetated, urban, or agricultural land) using the MODIS land cover product from the corresponding year (see Fig. 1a). For each day, OMI pixels and

fire pixels were grouped into fire “events” such that adjacent OMI pixels containing fires were grouped together and rectangular regions were defined around each event (see Fig. 1b). Each event then represents all fire pixels in that location from a single day of observation, where the fire pixels are close enough to each other that the OMI spatial resolution cannot separately resolve their emissions.

The total mass emitted by each fire as measured by OMI was calculated as follows: total OMI tropospheric NO₂ columns for each event ($X_{\text{NO}_2,f}$) were obtained by averaging all columns in the rectangular region, weighted by pixel area, with the column standard deviation ($\sigma_{\text{NO}_2,f}$) equal to the weighted average of column standard deviations reported in the retrieval. OMI columns over the rectangular region were measured in a similar way for 60 days before and after the fire; the average of these columns yielded an event background NO₂ column ($X_{\text{NO}_2,b}$) with corresponding background column standard deviation ($\sigma_{\text{NO}_2,b}$). Columns containing MODIS fire detections were eliminated from the background average. The total mass of NO₂ emitted by the fire M_{NO_2} (in kg) was then given by

$$M_{\text{NO}_2} = (X_{\text{NO}_2,f} - X_{\text{NO}_2,b}) \times A_R \quad (4)$$

where A_R is the regional area. The standard deviation for M_{NO_2} is given by

$$\sigma_{\text{NO}_2} = (\sigma_{\text{NO}_2,f} - \sigma_{\text{NO}_2,b}) \times A_R \quad (5)$$

As FRP is the rate of radiative energy release (MJ s^{-1}), the next step in the analysis was to determine the time over which the measured mass of NO₂ had been emitted. The time for emitted NO₂ to clear the region (t_c) was derived using wind speed (w) and direction from NARR wind fields at 900 hPa (~ 1 km):

$$t_c = d_c w^{-1}, \quad (6)$$

where d_c is the distance from the center of the fire to the edge of the region along the wind direction. Standard error in d_c was assumed to be at least 2 km (twice the nominal resolution of a MODIS pixel) and for larger fires, was given as the standard error associated with measuring the center of the fire; the center was found as an average of all fire pixel locations for that fire, weighted by FRP. Uncertainties in wind speed and direction for individual data points were difficult to assess and quantify, although we examine the effects of alternate wind data sets and assumptions about plume height in the discussion below; percent standard error in t_c was assumed equal to percent standard error in d_c . For each event, dividing M_{NO_2} by t_c yielded a mass emission rate (MER) of NO₂ for the region, with percent standard error equal to percent standard error from t_c and M_{NO_2} , summed in quadrature. Summing pixel FRP for each land type yielded the total event FRP for each land type (in MJ), with standard error estimated at 30 %, between 15 % and 46 % as reported in Wooster et al. (2003).

Satellite observations of fire emissions will necessarily contain a mixture of fresh and aged smoke, due to the spatial resolution of the observing instrument. NO_x is a relatively short-lived species; observations and theoretical studies both support the notion that NO_x concentrations in a fire plume will decay with time due to the formation of nitric acid (HNO₃) and NO_x reservoir species such as peroxyacetyl nitrate (PAN) (e.g. Jacob et al., 1992; Mauzerall et al., 1998; Leung et al., 2007; Real et al., 2007; Alvarado et al., 2010). Thus, the aged smoke present in satellite observations will bias our measured ECs low. To evaluate this effect, we consider a 1-D model of a fire plume, assuming a constant wind speed along the dependent axis; horizontal diffusion and vertical distribution of emissions are neglected. We also assume first-order reaction kinetics for NO_x, governed by a rate constant k ; the lifetime is $\tau = k^{-1}$. The concentration of NO₂ as a function of distance from the fire is then:

$$C(x) = C_0 \exp(-kw^{-1}x), \quad (7)$$

where C_0 is the concentration immediately over the source (kg m^{-3} in our 1-D model) and x is the distance downwind from the source. Note that since we assume a constant wind speed, the age of the smoke at x is given by $t = w^{-1}x$. The satellite will observe all NO₂ between the source and some point x_0 which represents the edge of the satellite pixel, and the total mass observed is equal to the integral of NO₂ concentration from the origin to x_0 :

$$M_{\text{NO}_2} = \int_0^{x_0} C(x) dx = C_0 \int_0^{x_0} \exp(-kw^{-1}x) dx = C_0 w k^{-1} [1 - \exp(-kw^{-1}x_0)]. \quad (8)$$

Here, the clear time, t_c , is defined as the time required for transport from the source to the edge of the pixel: $t_c = w^{-1}x_0$. We also note that $C_0 x_0$ corresponds to the total mass that would be observed had no decay in NO₂ occurred; thus $C_0 x_0 t_c^{-1}$ is equal to the mass emission rate that would have been measured with no decay, or equivalently, the initial mass emission rate at the fire source, MER_{init} . We can thus rewrite our total mass observed equation as:

$$M_{\text{NO}_2} = C_0 x_0 t_c^{-1} k^{-1} [1 - \exp(-kt_c)] = \text{MER}_{\text{init}} \tau [1 - \exp(-\tau^{-1}t_c)]. \quad (9)$$

Dividing both sides by t_c yields our measured MER as a function of the initial MER, lifetime τ , and clear time t_c :

$$\text{MER}_{\text{meas}} = \text{MER}_{\text{init}} \tau t_c^{-1} [1 - \exp(-\tau^{-1}t_c)]. \quad (10)$$

Although this 1-D model neglects diffusion, in most cases the width of the rectangular region is large enough that horizontal diffusion does not remove the fire-emitted NO₂ from

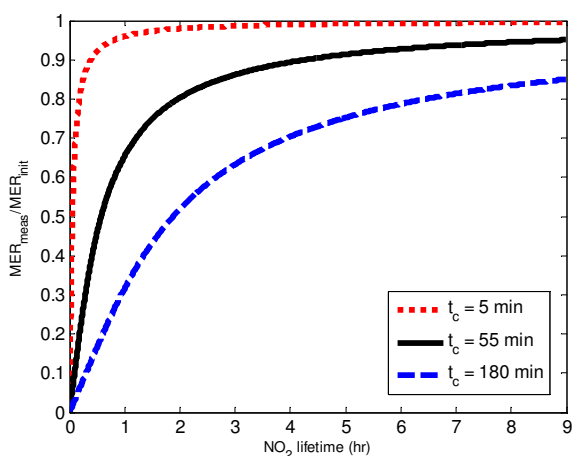


Fig. 2. The NO₂ mass emission rate (MER) measured in this analysis (as a fraction of the initial MER from the fire) vs. NO_x lifetime in the plume (Eq. 10) for three sample clear times in our analysis: the shortest (5 min), average (55 min) and longest (180 min).

the satellite field of view; thus this is a useful first order approximation of the relationship between initial and measured MER. We use this equation to apply a chemistry correction factor to each point in our analysis, assuming an appropriate lifetime.

Previous studies offer a range of NO_x lifetimes within fire plumes. Analyses have converged on lifetimes of less than 7 h with observationally constrained lifetimes closer to 2–3 h (Jacob et al., 1992; Yokelson et al., 1999; Alvarado et al., 2010). We select a lifetime of 2 h, which is in agreement with observations. A plot of MER decay for three different clear times (the time required to exit the satellite pixel) is shown in Fig. 2. These three clear times (5 min, 55 min, and 3 h) represent a short, average, and long clear time for our analysis, respectively. At a lifetime of 2 h, the apparent MER that would be inferred from the satellite observations for the average case is biased low by 20 %. Longer lifetimes result in less bias. Thus our choice of lifetime introduces at most a minor bias unless the lifetime is shorter than 45 min. We apply the correction to each point as a function of clear time, and assume an uncertainty from this correction equal to the percent difference between the measured and corrected MERs; overall uncertainty in the corrected MER is then obtained by summing in quadrature this uncertainty with the measured MER uncertainty.

To ensure that only high quality observations were included in the analysis, all events with a background column greater than 3.5×10^{15} molecules cm⁻² were omitted from further analysis as it was difficult to distinguish fire emissions from variations in the NO_x background (361 points). Events with a clear time of greater than 3 h were removed to reduce errors associated with changes in FRP or wind speed and direction during the transit time (199 points from the remaining dataset). Events from a region near Santa Barbara

(34–35° N, 118–121° W) were also removed, due to errors in wind over this region that are likely associated with unresolved Santa Ana winds (37 points). Finally, points that had both high percent uncertainty (>100 %) and high absolute uncertainty (>1 kg s⁻¹) in MER were removed (430 points); this preserved points with MER near zero and a high percent uncertainty but low overall uncertainty. Overall, 34 % of data points were removed via filtering; 1960 events remained for this analysis.

We identified several aspects of the study by Ichoku and Kaufman (2005) that did not translate to the OMI NO₂ observations. The method used by Ichoku and Kaufman (2005) to measure total and background mass overestimated emitted NO₂ when applied to our dataset, due to regional variation in NO_x concentrations on the spatial scale of an OMI pixel; hence our development of the method described above to account for these variations. This method analyzes several pixels at once, so there was also no need to include an averaging step at the end of the analysis. We also use a more precise determination of the characteristic length using the direction of the wind and the center of the fire, as well as a higher resolution wind dataset (NARR at 32 km resolution instead of the NCEP global reanalysis at 2° × 2.5°). The study presented by Ichoku and Kaufman (2005) performed regional and subregional analyses over the globe, and assumed these subregions were representative of a single fuel type; we instead applied the MODIS Land Cover product to individual fire pixels. Finally, our correction to account for photochemical processing is necessary for NO_x but was not needed in the original study by Ichoku and Kaufman (2005).

4 Results and discussion

Figure 3 shows FRP vs. MER for all fires, as well as fires separated by their primary fuel type. Fires were identified as forest, grass, or shrub fires if at least 75 % of FRP came from fire pixels of that fuel type. Best fit lines (with intercept fixed at zero) and R^2 values are shown. Distinctly different slopes are measured for all three fuel types, and with the exception of forest fires, analyzing emissions separated by fuel type improves the correlation coefficient. Forest fires exhibit more variability in emissions than other fuel types; this may be due to variations in the extent to which trees contribute to the fuel in forest-type fire pixels as opposed to underbrush and leaf litter, or greater variation in extent of flaming combustion during which most NO_x is emitted. The small number of larger fires (only four fires with FRP >5000 MJ) may also have an effect, as percent uncertainty in FRP is likely greater for small fires (Kaufman et al., 1998).

Limiting the analysis to individual fuel types reduces its statistical rigor. To obtain ECs with well-characterized uncertainties and including all of the data deemed reliable, a multiple regression with nonparametric bootstrap resampling was used. Since the emission parameterization scales

Table 1. NO₂ and NO_x ECs and NO_x EFs by fuel type.

Land type	NO ₂ EC (g MJ ⁻¹)	NO _x EF (g kg ⁻¹) ^{a,b}	NO _x EC (g MJ ⁻¹) ^a
Forest	0.279±0.077	0.59±0.16	0.243±0.067
Grass	0.342±0.053	0.73±0.11	0.297±0.046
Shrub	0.696±0.088	1.48±0.19	0.605±0.077

Reported uncertainties are 1σ, calculated via nonparametric bootstrap resampling.

^a assumes NO₂/NO_x of 0.75. Total NO_x mass expressed as NO.

^b assumes K_R = 0.41 kg MJ⁻¹.

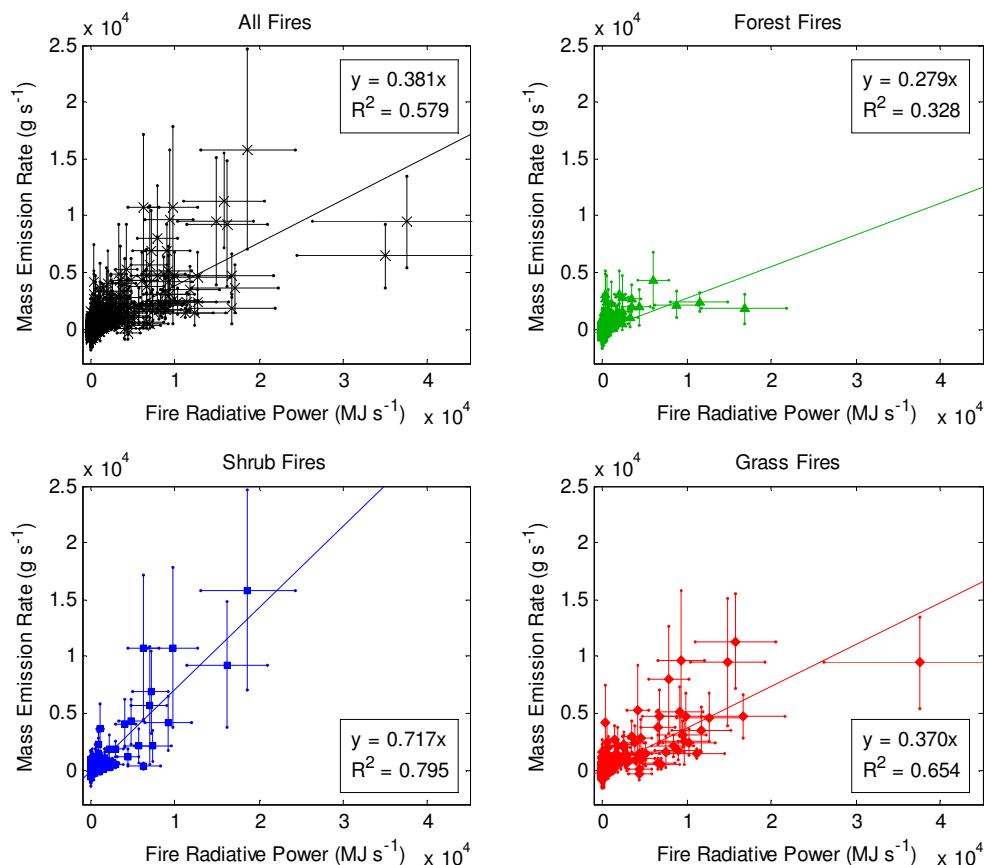


Fig. 3. Plots of fire radiative power (FRP) vs. NO₂ mass emission rate (MER) for fires grouped by land type: all (a), forests (b), shrubs (c), and grasses (d), with lines of best fit and R² values. Error bars are one standard deviation for MER and range for FRP as reported in the text.

linearly, the MER equation can be expanded to vary linearly with landtype:

$$\text{MER} = (\text{FRP}_F \times \text{EC}_F) + (\text{FRP}_G \times \text{EC}_G) + (\text{FRP}_S \times \text{EC}_S) \quad (11)$$

where F, G and S correspond to forest, grass and shrub land types. Points were randomly sampled with replacement and the multiple regression on land type FRP was performed 300 000 times; the resulting averaged ECs (in g MJ⁻¹ NO₂) and their standard deviations (Table 1) were used to calculate predicted MERs for each fire measured in the analysis,

as shown in Fig. 4. The best fit line (slope of 0.988) demonstrates that these ECs appropriately reproduce overall emissions. The correlation coefficient indicates that this parameterization method accounts for approximately 67% of the variability in emissions on this scale.

Previously, NO_x EFs of 2.5±1.2 for forests, 3.5±0.9 for grass and 6.5±2.7 (g kg⁻¹) for shrubs were reported for fires in North America by Battye and Battye (2002). As a ratio to the forest fire emissions, these reported NO_x EFs are 2.4 times higher for shrub fires and 1.6 for grass fires, mainly

Table 2. Possible biases in this analysis.

Possible biases	Bias range (%)	Bias direction
Assumed NO _x lifetime	0–20	Indeterminate
NO ₂ /NO _x ratio	0–20	Indeterminate
Value for <i>K</i>	0–15	Indeterminate
FRP overestimation due to diurnal fire cycle	15–20	Negative
Plume injection height assumptions	0–50	Negative
FRP underestimation due to clouds/smoke/canopy	15–30	Positive
Increased flaming sampling due to diurnal fire cycle	0–40	Positive
Emissions from CA/NV are lower than global average	Indeterminate	Indeterminate
Bias in OMI retrieval	Indeterminate	Indeterminate

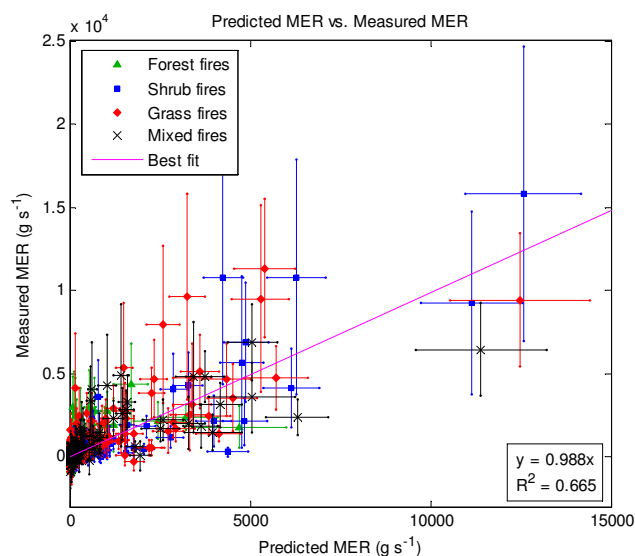


Fig. 4. Predicted NO₂ mass emission rate (MER), calculated using fire radiative power and the multiple regression coefficients, vs. MER measured in the analysis. Error bars in measured MER are one standard deviation, calculated as reported; error bars in predicted MER are calculated using one standard deviation of each calculated emission coefficient.

reflecting differences in the C:N ratios of the fuels and differences in typical combustion efficiency. Our analysis gives ECs that are 2.5 times larger for shrub fires and 1.2 times larger for grass fires than forest fires, consistent with those reported by Battye and Battye (2002). Globally averaged NO_x EFs presented in Andreae and Merlet (2001) do not include a shrub category, but the ratio of the grassland EF to the extratropical forest EF is 1.3 to 1; the grassland number was later revised down by 40 % (Hoelzemann et al., 2004), however, a number of papers have provided evidence that the extratropical forest EF should also be revised downward (Spichtinger et al., 2001; Cook et al., 2007; Alvarado et al., 2010).

To directly compare to previously reported NO_x ECs and EFs, we can convert using a photostationary state NO/NO₂

ratio and the aforementioned proportionality constant *K*, the ratio of biomass burned to FRE. For this comparison we assume that 75% of NO_x in the plume is present as NO₂, as the vast majority of fire plumes observed at OMI resolution are aged long enough for NO and NO₂ to reach photostationary state. This value is also consistent with previous observed and modeled values in fire plumes (Laursen et al., 1992; Alvarado and Prinn, 2009). We estimate that this value is accurate to within 20 %. We also use $K = 0.41 \text{ kg MJ}^{-1}$, the average of two values measured in previous studies (Wooster et al., 2005; Freeborn et al., 2008). This value was used in Vermote et al. (2009) and the uncertainty estimated to be at least 10 %. The resulting NO_x EFs and ECs are presented in Table 1, in g NO_x (as NO); we note that the overall bias induced by these conversions may be as high as 25 % in either direction.

Most reported NO_x emission factors are substantially larger than the ones we derive here. The NO_x EFs reported by Battye and Battye (2002) are roughly 3 times larger than our derived EFs. The grassland EF (2.32 g kg^{-1}) revised from Andreae and Merlet (2001) and given in Hoelzemann et al. (2004) is also roughly 3 times larger than our reported grassland EF and the extratropical forest EF (3.0 g kg^{-1}) from Andreae and Merlet (2001) is 5 times larger than our reported forest EF. Alvarado et al. (2010) used observations of NO_x in boreal forest fire plumes to obtain an emission factor for NO_x of 1.06 g kg^{-1} , almost twice our extratropical forest EF, with a reported uncertainty of $\sim 100\%$. Freeborn et al. (2008) report an overall NO_x EC of $1.19 \pm 0.65 \text{ g MJ}^{-1}$ for laboratory fires of a number of different fuel types, 2–5 times greater than the NO_x ECs measured in this work ($0.243\text{--}0.605 \text{ g MJ}^{-1}$).

A number of factors may be responsible for a bias in our measured values; these factors are presented in Table 2, and we discuss them here at length. First, we note that any assumptions we made about average fire behavior, such as NO_x lifetime within the plume, NO₂/NO_x ratio, or the value for *K*, are a possible source of systematic error, with under- and overestimation being equally likely; however, each of these sources is expected to induce less than 20 % error unless a

typical NO_x lifetime in a fire plume is less than 1 h. A second source of systematic error is the diurnal cycle of fire behavior. A number of studies indicate that fire activity peaks in the afternoon (Giglio, 2007; Zhang and Kondragunta, 2008; Vermote et al., 2009). Data presented in Vermote et al. (2009) and Zhang and Kondragunta (2008) suggests that average activity increases roughly linearly from morning to peak activity. Our analysis assumes constant FRP throughout the time over which emissions were measured for each data point; while some fires will increase in FRP over this time and some fires will decrease, the diurnal cycles presented in these studies suggest that on average we are overestimating FRP by up to 20 %, depending on the average clear time.

To verify this effect, we tested all points in our analysis that were also detected during the morning overpass of MODIS on the Terra satellite, approximately 25 % of the fires we studied, including the majority of large fires. For each point, we assumed FRP varied linearly from the Terra overpass to the Aqua overpass, and using the clear time, calculated the average FRP over the time of our measurement. Bootstrapping with these average FRPs instead of the Aqua FRP resulted in shrub and grass EFs approximately 15 % greater than those presented in this work, indicating a small low bias. The forest EF increased by 40 %, a much larger effect, but it is not clear that this is statistically significant.

Another potential source of bias is from the use of NARR data at the selected wind level (900 hPa). Plume height varies significantly between individual fires; 900 hPa, which corresponds to approximately 1 km altitude, was selected as a result of data presented by val Martin et al. (2010) indicating that average fire plume heights in North America are less than 1 km, and that the majority of fire plumes remain within the boundary layer. As a result, we expect wind level selection to induce some random error for individual fires, but the choice should be appropriate for an average fire. However, any bias in NARR wind speed at this level would result in a bias in this work. Additionally, val Martin et al. (2010) note a correlation with plume height and measured FRP, although the correlation is weak and the relationship may not be applicable to our analysis since the data presented in the study was obtained in the morning as opposed to the early afternoon, when meteorology governing plume injection height is very different. Still, increases in injection height with FRP could induce a bias in our results due to differences in wind speeds through the troposphere. However, even when fire plumes inject emissions to heights of a few kilometers, the vertical distribution of emissions is not well known (val Martin et al., 2010); the majority of emissions may remain in the boundary layer.

We performed three separate tests to determine the magnitude of any possible bias due to wind selection. First, we repeated the analysis using 850 hPa wind (~1.5 km altitude) from NARR. Obtained NO₂ EC values were within 0.020 g MJ⁻¹ of the values obtained using 900 hPa wind, less than a 10 % change and well within our reported uncertain-

ties. We concluded that small changes in wind level do not significantly bias the results. In the second test, we repeated the analysis using wind at 850 hPa from the NCEP Climate Forecast System Reanalysis, a global reanalysis and forecast produced at 0.5°×0.5° resolution (Saha et al., 2010). Differences in NO₂ EC values calculated via the two data sets were all less than 0.070 g MJ⁻¹ and again were within the reported uncertainties for all three land types. This test ensured that there is no large bias as a result of using NARR values instead of an alternative reanalysis. Finally, we performed the analysis again using NARR wind at 700 hPa (~3 km) for fires with FRP greater than 5000 MJ s⁻¹ and NARR wind at 900 hPa for smaller fires. Due to increased wind speeds with increasing altitude in the troposphere, the use of this higher wind resulted in an increase in NO₂ ECs for all three land types, ranging from 20 % to 50 %. Thus we consider our assumption of plume injection height a possible source of negative bias.

There are also some sources of systematic error that would bias our EFs high, including underestimation of FRP by MODIS due to clouds, smoke or canopy cover obscuring the satellite view of radiant fire energy (Vermote et al., 2009). The absence of coincident measurements of FRP from satellite and ground or airborne platforms prevents direct assessment of this uncertainty; however, OMI pixels used in this analysis are filtered for cloud fraction >20 %, largely eliminating fires that are partially obscured by clouds, or aerosol interpreted by the retrieval as cloud. We also note that comparison between FRP from other satellite platforms and FRP from MODIS suggests that when an individual fire is detected by both instruments, measured FRP is accurate to within 45 %. For example, Roberts et al. (2005) compare FRP from MODIS to FRP derived from the Spinning Enhanced Visible and Infrared Imager (SEVIRI) instrument, and find that for fires in Southern Africa detected by both instruments, the average underestimation by SEVIRI (which is less sensitive to pixels with low FRP) is 5 %. Similarly, Wooster et al. (2003) indicate that MODIS-derived FRE differed by ~15–45 % from FRE derived from the Bi-spectral InfraRed Detection (BIRD) satellite for fires detected by both instruments, with an average underestimation by MODIS of ~15 % for all individually compared fires. Since the BIRD measurements are higher spatial resolution and expected to observe fires more accurately, this suggests an average underestimation of FRP of no more 15–30 % in the MODIS product.

There is other evidence for underestimation of total regional FRP based on the MODIS retrieval. Some biomass burned and fire emission inventories have been developed using FRP (e.g. Ellicott et al., 2009; Vermote et al., 2009) and these generally indicate that biomass burned derived from MODIS FRP are lower than estimates of biomass burned using GFEDv2, possibly by up to a factor of 3. Other studies indicate that biomass burned from GFEDv2 could be underestimated itself (e.g. Kopacz et al., 2010; Lioussé et al.,

2010), indicating a possible underestimation in MODIS estimates of total regional FRP that could be significant. However, it is likely that these discrepancies are largely due to omission of small fires that are either completely obscured by clouds or not detected by the MODIS algorithm which has limited sensitivity to pixels with low FRP. This effect was observed in the aforementioned studies: Roberts et al. (2005) noted a much larger underestimation in FRP of 38 % by SEVIRI (which is not as sensitive as MODIS to fires with FRP < 100 MW) relative to MODIS when comparing total regional FRP measurements. Wooster et al. (2003) also observed that total regional MODIS FRP was only ~60 % of total regional BIRD FRP, despite 15 % average differences for individual fire comparisons. Our analysis evaluates emissions of individual detected fires to derive ECs; consequently, our conclusions are insensitive to fires that are too small to be detected and uncertainties specific to total regional FRP do not affect our results. However, the application of these ECs to predict total emissions in a region (as opposed to emission from a specific fire) will require evaluation of the contribution of fires that are undetected by MODIS to the total emissions.

It is also possible that since our observations occur close to the peak in fire activity, the fires we observe may be more heavily weighted towards flaming emissions than an average wildfire, and thus are biased high. This uncertainty is difficult to quantify, since precise measurements of diurnal patterns in NO_x emission factors have not yet been performed. In addition, the diurnal pattern in wildfire flaming to smoldering fraction is not established, and while NO_x emissions are correlated with flaming combustion and higher modified combustion efficiency (MCE), this correlation is small – $R^2 = 0.11$ in Battye and Battye (2002) – and the slope of the line very uncertain. However, MCE for most fires ranges between 0.80 and 1.0 (McMeeking et al., 2009; Yokelson et al., 2008; Battye and Battye, 2002) and thus any diurnal change in average MCE would likely be well within this range. Using the Battye and Battye (2002) fit despite the weak correlation, we determine that for changes in average MCE from 0.95 to 0.90, there is a 30 % decrease in NO_x EF; for changes in average MCE from 0.90 to 0.85, there is a 40 % decrease in NO_x EF. This is consistent when compared to seasonal variations in NO_x emission ratios presented by Lapina et al. (2008), who attribute the observed seasonal change in emission ratio of NO_y to CO for boreal forests, from 7.3 mol mol⁻¹ to 2.8 mol mol⁻¹, to higher smoldering fraction in the late-season fires. In order to translate these values to differences in NO_x EFs, the increase in CO emissions with increasing smoldering fraction must be accounted for. Unfortunately, Lapina et al. (2008) do not report MCE for the fires, but using equations presented in Battye and Battye (2002), a decrease in MCE from 0.95 to 0.90 results in a factor of ~2.3 increase in the CO emission factor (from 45.6 g kg⁻¹ to 103 g kg⁻¹); a decrease from 0.90 to 0.85 results in a factor of ~1.5 increase. If these CO emission factors are used with the NO_y

emission ratios from Lapina et al. (2008) to calculate NO_x EFs, then the seasonal decrease in NO_x EF inferred from the reported data would be 15–40 %. Thus, while it is currently impossible to accurately quantify the potential bias induced by this diurnal variation in NO_x EF, we suggest that the bias is at most 40 %.

A summary of all quantified potential biases is presented in Table 2, in the first seven rows. Summing these biases suggests that our values are nearly equally likely to be biased high or low (likely bias ranging from approximately 55 % low to 55 % high). In addition, these potential biases cannot entirely account for the discrepancy between our emission coefficients and prior estimates.

We might interpret these results to indicate that there is a bias in the OMI retrieval process over wildfires. The NO₂ tropospheric column retrieval does not account for specific temporal differences in NO₂ vertical profile and aerosol loading associated with wildfire conditions, nor does it explicitly account for effects of aerosol loading due to fires, both of which can act to systematically bias NO₂ columns over wildfires. Most analyses suggest the bias due to aerosol is relatively minor (<20 %), as aerosol is treated implicitly as part of the cloud correction (Boersma et al., 2004). Uncertainty due to profile shape is more difficult to constrain, as NO₂ profile data is sparse; Lamsal et al. (2010) indicate that biases between the OMI standard product and ground based measurements range from –5.6 % to 71 %, and they attribute much of this difference to profile error. Unfortunately, any bias in this work cannot be assessed using data from another NO₂ remote sensing platform e.g. SCIAMACHY, due to differences in overpass times and spatial coverage, lower spatial resolution, or the fact that these instruments generally use a similar retrieval process and so may be subject to similar biases. Simultaneous in situ and satellite observation of NO₂ in plumes would be extremely useful as a constraint. Despite our inability to quantify the contributions to the values presented in this work, we include a bias in the OMI retrieval in Table 2.

Another possibility is that emissions from wildfires in California are lower than emissions used to derive prior estimates. However, this is not observed in previous measurements of emissions (e.g. Battye and Battye, 2002). Our own preliminary analysis of global measurements using the methods outlined in this paper also provides no evidence that CA/NV fires are uniquely different from fires in other geographic locations. Nonetheless, we include this in Table 2 as a potential source of bias to be thorough.

A third possible explanation for the difference is that previous in situ and laboratory studies overestimate NO_x emissions from wildfires, due to oversampling of flaming emissions in the laboratory or from airborne platforms. There is evidence that laboratory and airborne emission measurements sample plumes with higher MCE and greater NO_x emissions than ground stations (e.g. Yokelson et al., 2008). These low-level smoldering emissions have been suggested

to contribute only very minimally to total fire emissions (Andreae and Merlet, 2001); however, if smoldering combustion contributes more significantly to overall emissions than previously suggested, that would result in an overestimation of EFs of species associated with flaming combustion (e.g. NO_x) when these EFs are measured via airborne platforms and then applied to large-scale fires. We note that results from other studies producing ECs for aerosol using satellite data are consistent with this hypothesis (Ichoku and Kaufman, 2005; Vermote et al., 2009); aerosol is more strongly emitted during smoldering combustion, and both of the aforementioned studies measure higher aerosol emissions than are represented by currently accepted aerosol EFs. Kopacz et al. (2010) constrain CO emission sources using data from several satellite platforms, and find that wildfire emissions as a source of CO are underestimated using GFEDv2 emissions. While Kopacz et al. (2010) conclude that GFEDv2 biomass burned is underestimated, other studies suggest that GFEDv2 biomass burned may be overestimated (e.g. Ellicott et al., 2009), and the result in Kopacz et al. (2010) may also be consistent with the hypothesis that current EFs underestimate contributions of smoldering combustion, as emissions of both CO and hydrocarbons that oxidize rapidly to CO are associated with smoldering combustion. The support of this hypothesis across studies that measure different species, emitted during different stages of combustion, and across different satellite platforms is remarkably consistent. We recommend that a more systematic study of smoldering and flaming combustion as they pertain to wildfire emissions be conducted, and conclude that the NO_x ECs and EFs presented here are a useful lower bound on NO_x emissions and, if the contribution of smoldering combustion to total wildfire emissions is indeed underestimated, may provide a more accurate characterization of fire emissions than currently used values.

5 Conclusions

We derive NO₂ ECs (in g MJ⁻¹ NO₂) for wildfires in California and Nevada using satellite measurements of NO₂ column densities and fire radiative energy. ECs for forest, grass and shrub fuels were found to be 0.279±0.077, 0.342±0.053, and 0.696±0.088 g MJ⁻¹ NO₂, respectively, with reported uncertainties equal to the standard deviation in the measurement. The variation of these ECs with land type reproduces ratios seen in previous work; however, these ECs are significantly lower than previously reported emissions estimates. Systematic biases in assumptions within the analysis and in FRP measurement cannot fully account for these differences. We conclude that there may be a large (50–100 %) negative bias in the OMI retrieval of NO₂ columns over wildfire plumes, presumably due to errors in assumed profile shape. However, comparison of our results with those of Ichoku and Kaufman (2005), Vermote et al. (2009), and Kopacz et

al. (2010) also indicates that previously reported NO_x EFs are likely overestimated, due to oversampling of flaming combustion by laboratory and airborne measurements. Regardless of the contributions of these factors, the parameters derived here are unambiguously a lower bound on fire NO_x emissions.

Acknowledgements. This work was supported by the National Aeronautics and Space Administration, grant NNX08AE566, and by an award from the Department of Energy (DOE) Office of Science Graduate Fellowship Program (DOE SCGF). The DOE SCGF Program was made possible in part by the American Recovery and Reinvestment Act of 2009. The DOE SCGF program is administered by the Oak Ridge Institute for Science and Education (ORISE) for the DOE. ORISE is managed by Oak Ridge Associated Universities (ORAU) under DOE contract number DE-AC05-06OR23100. All opinions expressed in this paper are the authors' and do not necessarily reflect the policies and views of DOE, ORAU, or ORISE. OMI data used in this effort were acquired as part of the activities of NASA's Science Mission Directorate, and are archived and distributed by the Goddard Earth Sciences (GES) Data and Information Services Center (DISC). MODIS data are distributed by the Land Processes Distributed Active Archive Center (LP DAAC), located at the US Geological Survey (USGS) Earth Resources Observation and Science (EROS) Center (<http://lpdaac.usgs.gov>). NARR data were obtained through the NOAA National Operational Model Archive & Distribution System (NOMADS).

Edited by: A. Richter

References

- Alvarado, M. J. and Prinn, R. G.: Formation of ozone and growth of aerosols in young smoke plumes from biomass burning: 1. Lagrangian parcel studies, *J. Geophys. Res.*, 114, D09306, doi:10.1029/2008JD011144, 2009.
- Alvarado, M. J., Logan, J. A., Mao, J., Apel, E., Riemer, D., Blake, D., Cohen, R. C., Min, K.-E., Perring, A. E., Browne, E. C., Wooldridge, P. J., Diskin, G. S., Sachse, G. W., Fuelberg, H., Sessions, W. R., Harrigan, D. L., Huey, G., Liao, J., Case-Hanks, A., Jimenez, J. L., Cubison, M. J., Vay, S. A., Weinheimer, A. J., Knapp, D. J., Montzka, D. D., Flocke, F. M., Pollack, I. B., Wennberg, P. O., Kurten, A., Crouse, J., Clair, J. M. St., Wisthaler, A., Mikoviny, T., Yantosca, R. M., Carouge, C. C., and Le Sager, P.: Nitrogen oxides and PAN in plumes from boreal fires during ARCTAS-B and their impact on ozone: an integrated analysis of aircraft and satellite observations, *Atmos. Chem. Phys.*, 10, 9739–9760, doi:10.5194/acp-10-9739-2010, 2010.
- Andreae, M. O. and Merlet, P.: Emission of trace gases and aerosols from biomass burning, *Global Biogeochem. Cy.*, 15, 955–966, 2001.
- Battye, W. and Battye, R.: Development of emissions inventory methods for wildland fire, US Environmental Protection Agency, Research Triangle Park, NC, USA, Contract 68-D-98-046, 2002.
- Boersma, F., Bucsela, E., Brinksma, E., and Gleason, J. F.: NO₂, in: OMI Algorithm Theoretical Basis Document, Vol. IV: OMI

- Trace Gas Algorithms, 2, edited by: Chance, K., Smithsonian Astrophysical Observatory, Cambridge, MA, USA, 13–36, 2002.
- Boersma, K. F., Eskes, H. J., and Brinkma, E. J.: Error analysis for tropospheric NO₂ retrieval from space, *J. Geophys. Res.-Atmos.*, 109, D04311, doi:10.1029/2003JD003962, 2004.
- Bucsele, E. J., Celarier, E. A., Wenig, M. O., Gleason, J. F., Veefkind, J. P., Boersma, K. F., and Brinkma, E. J.: Algorithm for NO₂ vertical column retrieval from the ozone monitoring instrument, *IEEE Trans. Geosci. Remote Sens.*, 44, 1245–1258, 2006.
- Celarier, E. A., Brinkma, E. J., Gleason, J. F., Veefkind, J. P., Cede, A., Herman, J. R., Ionov, D., Goutail, F., Pommereau, J. P., Lambert, J. C., van Roozendaal, M., Pinardi, G., Wittrock, F., Schonhardt, A., Richter, A., Ibrahim, O. W., Wagner, T., Bojkov, B., Mount, G., Spinei, E., Chen, C. M., Pongetti, T. J., Sander, S. P., Bucsele, E. J., Wenig, M. O., Swart, D. P. J., Volten, H., Kroon, M., and Levelt, P. F.: Validation of ozone monitoring instrument nitrogen dioxide columns, *J. Geophys. Res.*, 113, D15S15, doi:10.1029/2007JD008908, 2008.
- Cook, P. A., Savage, N. H., Turquety, S., Carver, G. D., O'Connor, F. M., Heckel, A., Stewart, D., Whalley, L. K., Parker, A. E., Schlager, H., Singh, H. B., Avery, M. A., Sachse, G. W., Brune, W., Richter, A., Burrows, J. P., Purvis, R., Lewis, A. C., Reeves, C. E., Monks, P. S., Levine, J. G., and Pyle, J. A.: Forest fire plumes over the North Atlantic: p-TOMCAT model simulations with aircraft and satellite measurements from the ITOP/ICARTT campaign, *J. Geophys. Res.*, 112, D10S43, doi:10.1029/2006JD007563, 2007.
- Denman, K. L., Brasseur, A., Chidthaisong, A., Ciais, P., Cox, P. M., Dickinson, R. E., Hauglustaine, D., Heinze, C., Holland, E., Jacob, D., Lohmann, U., Ramachandran, S., da Silva Dias, P. L., Wofsy, S. C., and Zhang, X.: Couplings Between Changes in the Climate System and Biogeochemistry, in: *Climate Change 2007: The Physical Science Basis, Contribution of Working Group I to the Fourth Assessment Report of the Intergovernmental Panel on Climate Change*, edited by: Solomon, S., Qin, D., Manning, M., Chen, Z., Marquis, M., Averyt, K. B., Tignor, M., and Miller, H. L., Cambridge University Press, Cambridge, UK and New York, NY, USA, 499–588, 2007.
- Ellicott, E., Vermote, E., Giglio, L., and Roberts, G.: Estimating biomass consumed from fire using MODIS FRE, *Geophys. Res. Lett.*, 36, L13401, doi:10.1029/2009GL038581, 2009.
- Freeborn, P. H., Wooster, M. J., Hao, W. M., Ryan, C. A., Nordgren, B. L., Baker, S. P., and Ichoku, C.: Relationships between energy release, fuel mass loss, and trace gas and aerosol emissions during laboratory biomass fires, *J. Geophys. Res.*, 113, D01301, doi:10.1029/2007JD008679, 2008.
- Friedl, M. A., Sulla-Menashe, D., Tan, B., Schneider, A., Ramankutty, N., Sibley, A., and Huang, X. M.: MODIS Collection 5 global land cover: Algorithm refinements and characterization of new datasets, *Remote Sens. Environ.*, 114, 168–182, 2010.
- Giglio, L.: Characterization of the tropical diurnal fire cycle using VIRS and MODIS observations, *Remote Sens. Environ.*, 108, 407–421, 2007.
- Giglio, L., Descloitres, J., Justice, C. O., and Kaufman, Y. J.: An enhanced contextual fire detection algorithm for MODIS, *Remote Sens. Environ.*, 87, 273–282, 2003.
- Goode, J. G., Yokelson, R. J., Susott, R. A., and Ward, D. E.: Trace gas emissions from laboratory biomass fires measured by open-path Fourier transform infrared spectroscopy: Fires in grass and surface fuels, *J. Geophys. Res.-Atmos.*, 104, 21237–21245, 1999.
- Goode, J. G., Yokelson, R. J., Ward, D. E., Susott, R. A., Babbitt, R. E., Davies, M. A., and Hao, W. M.: Measurements of excess O₃, CO₂, CO, CH₄, C₂H₄, C₂H₂, HCN, NO, NH₃, HCOOH, CH₃COOH, HCHO, and CH₃OH in 1997 Alaskan biomass burning plumes by airborne fourier transform infrared spectroscopy (AFTIR), *J. Geophys. Res.*, 105, 22147–22166, 2000.
- Hoelzemann, J. J., Schultz, M. G., Brasseur, G. P., Granier, C., and Simon, M.: Global Wildland Fire Emission Model (GWEM): Evaluating the use of global area burnt satellite data, *J. Geophys. Res.-Atmos.*, 109, D14S04, doi:10.1029/2003JD003666, 2004.
- Hudman, R. C., Murray, L. T., Jacob, D. J., Turquety, S., Wu, S., Millet, D. B., Avery, M., Goldstein, A. H., and Holloway, J.: North American influence on tropospheric ozone and the effects of recent emission reductions: Constraints from ICARTT observations, *J. Geophys. Res.*, 114, D07302, doi:10.1029/2008JD010126, 2009.
- Ichoku, C. and Kaufman, Y. J.: A method to derive smoke emission rates from MODIS fire radiative energy measurements, *IEEE Trans. Geosci. Remote Sens.*, 43, 2636–2649, 2005.
- Jacob, D. J., Wofsy, S. C., Bakwin, P. S., Fan, S. M., Harriss, R. C., Talbot, R. W., Bradshaw, J. D., Sandholm, S. T., Singh, H. B., Browell, E. V., Gregory, G. L., Sachse, G. W., Shipham, M. C., Blake, D. R., and Fitzjarrald, D. R.: Summertime Photochemistry of the Troposphere at High Northern Latitudes, *J. Geophys. Res.*, 97, 16421–16431, 1992.
- Jaeglé, L., Steinberger, L., Martin, R. V., and Chance, K.: Global partitioning of NO_x sources using satellite observations: Relative roles of fossil fuel combustion, biomass burning and soil emissions, *Faraday Disc.*, 130, 407–423, 2005.
- Jordan, N. S., Ichoku, C., and Hoff, R. M.: Estimating smoke emissions over the US Southern Great Plains using MODIS fire radiative power and aerosol observations, *Atmos. Environ.*, 42, 2007–2022, 2008.
- Justice, C. O., Giglio, L., Korontzi, S., Owens, J., Morisette, J. T., Roy, D., Descloitres, J., Alleaume, S., Petitcolin, F., and Kaufman, Y.: The MODIS fire products, *Remote Sens. Environ.*, 83, 244–262, 2002.
- Kaufman, Y. J., Justice, C. O., Flynn, L. P., Kendall, J. D., Prins, E. M., Giglio, L., Ward, D. E., Menzel, W. P., and Setzer, A. W.: Potential global fire monitoring from EOS-MODIS, *J. Geophys. Res.*, 103, 32215–32238, 1998.
- Kopacz, M., Jacob, D. J., Fisher, J. A., Logan, J. A., Zhang, L., Megretskaia, I. A., Yantosca, R. M., Singh, K., Henze, D. K., Burrows, J. P., Buchwitz, M., Khlystova, I., McMillan, W. W., Gille, J. C., Edwards, D. P., Eldering, A., Thouret, V., and Nedelec, P.: Global estimates of CO sources with high resolution by adjoint inversion of multiple satellite datasets (MOPITT, AIRS, SCIAMACHY, TES), *Atmos. Chem. Phys.*, 10, 855–876, doi:10.5194/acp-10-855-2010, 2010.
- Lamsal, L. N., Martin, R. V., van Donkelaar, A., Celarier, E. A., Bucsele, E. J., Boersma, K. F., Dirksen, R., Luo, C., and Wang, Y.: Indirect validation of tropospheric nitrogen dioxide retrieved from the OMI satellite instrument: Insight into the seasonal variation of nitrogen oxides at northern midlatitudes, *J. Geophys. Res.-Atmos.*, 115, D05302, doi:10.1029/2009JD013351, 2010.

- Lapina, K., Honrath, R. E., Owen, R. C., Val Martin, M., Hyer, E. J., and Fialho, P.: Late summer changes in burning conditions in the boreal regions and their implications for NO_x and CO emissions from boreal fires, *J. Geophys. Res.*, 113, D11304, doi:10.1029/2007JD009421, 2008.
- Laursen, K. K., Hobbs, P. V., Radke, L. F., and Rasmussen, R. A.: Some Trace Gas Emissions from North-American Biomass Fires with an Assessment of Regional and Global Fluxes from Biomass Burning, *J. Geophys. Res.*, 97, 20687–20701, 1992.
- Leung, F. Y. T., Logan, J. A., Park, R., Hyer, E., Kasischke, E., Streets, D., and Yurganov, L.: Impacts of enhanced biomass burning in the boreal forests in 1998 on tropospheric chemistry and the sensitivity of model results to the injection height of emissions, *J. Geophys. Res.*, 112, D10313, doi:10.1029/2006JD008132, 2007.
- Lioussé, C., Guillaume, B., Gregoire, J. M., Mallet, M., Galy, C., Pont, V., Akpo, A., Bedou, M., Castra, P., Dungall, L., Gardrat, E., Granier, C., Konare, A., Malavelle, F., Mariscal, A., Mieville, A., Rosset, R., Serca, D., Solmon, F., Tummon, F., Assamoi, E., Yoboue, V., and Van Velthoven, P.: Updated African biomass burning emission inventories in the framework of the AMMA-IDAF program, with an evaluation of combustion aerosols, *Atmos. Chem. Phys.*, 10, 9631–9646, doi:10.5194/acp-10-9631-2010, 2010.
- Mauzerall, D. L., Logan, J. A., Jacob, D. J., Anderson, B. E., Blake, D. R., Bradshaw, J. D., Heikes, B., Sachse, G. W., Singh, H., and Talbot, B.: Photochemistry in biomass burning plumes and implications for tropospheric ozone over the tropical South Atlantic, *J. Geophys. Res.*, 103, 8401–8423, 1998.
- McMeeking, G. R., Kreidenweis, S. M., Baker, S., Carrico, C. M., Chow, J. C., Collett, J. L., Hao, W. M., Holden, A. S., Kirchstetter, T. W., Malm, W. C., Moosmuller, H., Sullivan, A. P., and Wold, C. E.: Emissions of trace gases and aerosols during the open combustion of biomass in the laboratory, *J. Geophys. Res.*, 114, D19210, doi:10.1029/2009JD011836, 2009.
- Mesinger, F., DiMego, G., Kalnay, E., Mitchell, K., Shafran, P. C., Ebisuzaki, W., Jovic, D., Woollen, J., Rogers, E., Berbery, E. H., Ek, M. B., Fan, Y., Grumbine, R., Higgins, W., Li, H., Lin, Y., Manikin, G., Parrish, D., and Shi, W.: North American regional reanalysis, *B. Am. Meteorol. Soc.*, 87, 343–360, 2006.
- Pfister, G. G., Wiedinmyer, C., and Emmons, L. K.: Impacts of the fall 2007 California wildfires on surface ozone: Integrating local observations with global model simulations, *Geophys. Res. Lett.*, 35, L19814, doi:10.1029/2008GL034747, 2008.
- Real, E., Law, K. S., Weinzierl, B., Fiebig, M., Petzold, A., Wild, O., Methven, J., Arnold, S., Stohl, A., Huntrieser, H., Roiger, A., Schlager, H., Stewart, D., Avery, M., Sachse, G., Browell, E., Ferrare, R., and Blake, D.: Processes influencing ozone levels in Alaskan forest fire plumes during long-range transport over the North Atlantic, *J. Geophys. Res.*, 112, D10S41, doi:10.1029/2006JD007576, 2007.
- Roberts, G., Wooster, M. J., Perry, G. L. W., Drake, N., Rebelo, L.-M., and Dipotso, F.: Retrieval of biomass combustion rates and totals from fire radiative power observations: Application to southern Africa using geostationary SEVIRI imagery, *J. Geophys. Res.*, 110, D21111, doi:10.1029/2005JD006018, 2005.
- Saha, S., Moorthi, S., Pan, H.-L., Wu, X., Wang, J., Nadiga, S., Tripp, P., Kistler, R., Woollen, J., Behringer, D., Liu, H., Stokes, D., Grumbine, R., Gayno, G., Wang, J., Hou, Y.-T., Chuang, H.-Y., Juang, H.-M. H., Sela, J., Iredell, M., Treadon, R., Kleist, D., Van Delst, P., Keyser, D., Derber, J., Ek, M., Meng, J., Wei, H., Yang, R., Lord, S., van den Dool, H., Kumar, A., Wang, W., Long, C., Chelliah, M., Xue, Y., Huang, B., Schemm, J.-K., Ebisuzaki, W., Lin, R., Xie, P., Chen, M., Zhou, S., Higgins, W., Zou, C.-Z., Liu, Q., Chen, Y., Han, Y., Cucurull, L., Reynolds, R. W., Rutledge, G., and Goldberg, M.: The NCEP Climate Forecast System Reanalysis, *B. Am. Meteorol. Soc.*, 91, 1015–1057, 2010.
- Seiler, W. and Crutzen, P. J.: Estimates of Gross and Net Fluxes of Carbon between the Biosphere and the Atmosphere from Biomass Burning, *Clim. Change*, 2, 207–247, 1980.
- Spichtinger, N., Wenig, M., James, P., Wagner, T., Platt, U., and Stohl, A.: Satellite detection of a continental-scale plume of nitrogen oxides from boreal forest fires, *Geophys. Res. Lett.*, 28, 4579–4582, 2001.
- Val Martin, M., Honrath, R. E., Owen, R. C., Pfister, G., Fialho, P., and Barata, F.: Significant enhancements of nitrogen oxides, black carbon, and ozone in the North Atlantic lower free troposphere resulting from North American boreal wildfires, *J. Geophys. Res.*, 111, D23S60, doi:10.1029/2006JD007530, 2006.
- Val Martin, M., Logan, J. A., Kahn, R. A., Leung, F.-Y., Nelson, D. L., and Diner, D. J.: Smoke injection heights from fires in North America: analysis of 5 years of satellite observations, *Atmos. Chem. Phys.*, 10, 1491–1510, doi:10.5194/acp-10-1491-2010, 2010.
- van Leeuwen, T. T. and van der Werf, G. R.: Spatial and temporal variability in the ratio of trace gases emitted from biomass burning, *Atmos. Chem. Phys.*, 11, 3611–3629, doi:10.5194/acp-11-3611-2011, 2011.
- Vermote, E., Ellicott, E., Dubovik, O., Lapyonok, T., Chin, M., Giglio, L., and Roberts, G. J.: An approach to estimate global biomass burning emissions of organic and black carbon from MODIS fire radiative power, *J. Geophys. Res.*, 114, D18205, doi:10.1029/2008JD011188, 2009.
- Wiedinmyer, C., Quayle, B., Geron, C., Belote, A., McKenzie, D., Zhang, X. Y., O'Neill, S., and Wynne, K. K.: Estimating emissions from fires in North America for air quality modeling, *Atmos. Environ.*, 40, 3419–3432, 2006.
- Wooster, M. J.: Small-scale experimental testing of fire radiative energy for quantifying mass combusted in natural vegetation fires, *Geophys. Res. Lett.*, 29, 2027, doi:10.1029/2002GL015487, 2002.
- Wooster, M. J., Zhukov, B., and Oertel, D.: Fire radiative energy for quantitative study of biomass burning: derivation from the BIRD experimental satellite and comparison to MODIS fire products, *Remote Sens. Environ.*, 86, 83–107, 2003.
- Wooster, M. J., Roberts, G., Perry, G. L. W., and Kaufman, Y. J.: Retrieval of biomass combustion rates and totals from fire radiative power observations: FRP derivation and calibration relationships between biomass consumption and fire radiative energy release, *J. Geophys. Res.*, 110, D24311, doi:10.1029/2005JD006318, 2005.
- Yokelson, R. J., Goode, J. G., Ward, D. E., Susott, R. A., Babbitt, R. E., Wade, D. D., Bertschi, I., Griffith, D. W. T., and Hao, W. M.: Emissions of formaldehyde, acetic acid, methanol, and other trace gases from biomass fires in North Carolina measured by airborne Fourier transform infrared spectroscopy, *J. Geophys. Res.-Atmos.*, 104, 30109–30125, 1999.

- Yokelson, R. J., Urbanski, S. P., Atlas, E. L., Toohey, D. W., Alvarado, E. C., Crouse, J. D., Wennberg, P. O., Fisher, M. E., Wold, C. E., Campos, T. L., Adachi, K., Buseck, P. R., and Hao, W. M.: Emissions from forest fires near Mexico City, *Atmos. Chem. Phys.*, 7, 5569–5584, doi:10.5194/acp-7-5569-2007, 2007.
- Yokelson, R. J., Christian, T. J., Karl, T. G., and Guenther, A.: The tropical forest and fire emissions experiment: laboratory fire measurements and synthesis of campaign data, *Atmos. Chem. Phys.*, 8, 3509–3527, doi:10.5194/acp-8-3509-2008, 2008.
- Zhang, X. Y. and Kondragunta, S.: Temporal and spatial variability in biomass burned areas across the USA derived from the GOES fire product, *Remote Sens. Environ.*, 112, 2886–2897, 2008.